


RESEARCH ARTICLE

Design, modeling and solar tracking control for a novel parabolic dish solar concentrator

Han Mo , Fanmao Liu, Cancan Liao and Yuanyuan Zhang

College of Mechanical and Electrical Engineering, Hunan University of Science and Technology, Xiangtan, Hunan, 411100, China

Corresponding author: Fanmao Liu; Email: liufanmao@hotmail.com

Received: 13 December 2022; **Revised:** 7 April 2023; **Accepted:** 28 May 2023; **First published online:** 26 June 2023

Keywords: Parabolic dish solar concentrator; 3-RPS parallel manipulator; Solar tracking; PSO-PID controller

Abstract

A novel parabolic dish solar concentrator based on the improved 3-RPS parallel manipulator to drive the reflective mirror facet is proposed and designed, which can not only automatically adjust the position and orientation of the reflective mirror facet but also have the advantages of independent drive, high stiffness and no cumulative error. Then, using the coordinate transformation matrixes of the novel parabolic dish solar tracking platform, the kinematics models of the 3-RPS parallel manipulators associated with the solar altitude and azimuth angles are established. The altitude and azimuth angles of the solar movement at the installation location are calculated according to the calculation formula of solar position. To solve the problem of too many telescopic rods of the 3-RPS parallel manipulator, a genetic algorithm is used to optimize the height of the concentrator's center of mass. Then the ideal trajectory and attitude of each telescopic rod of the 3-RPS parallel manipulators at different times of the day can be obtained with the inverse kinematics. The particle swarm optimization (PSO)-proportional-integral-derivative (PID) controller, which uses PSO algorithm to tune PID parameters, is proposed for solar trajectory tracking of the novel parabolic dish solar concentrator. The visual simulation model of the parabolic dish system is established in Simscape Multibody, and the trajectory tracking control experiment is carried out. The experimental results show that the trajectory tracking error of the novel dish solar tracking platform can be within 2.6 mm by using the PSO-PID controller.

1. Introduction

With the acceleration of the global industrialization process and the rapid development of the modern social economy, traditional fossil fuels have been consumed in large quantities, and the contradiction between energy shortages and environmental pollution is becoming increasingly significant. Improving the energy structure and increasing the proportion of clean energy in the consumption structure is one of the most urgent tasks for humanity. Solar energy is considered one of the most promising new energy sources because of its infinite, wide distribution and cleanliness characteristics. Among the numerous solar power generation technologies, dish solar thermal power generation technology has a good development prospect because of its advantages, such as the highest hot spot conversion efficiency and flexible use [1].

The dish solar thermal power generation system requires the normal of the concentrator to be parallel to the incident sunlight, so the design and control technology of the solar tracking mechanism is the key to realizing solar power generation in the dish system. At present, the structure of solar tracking mechanisms mainly includes single-axis, dual-axis and parallel mechanisms. The structure of the single-axis tracking mechanism is simple and easy to control, but the efficiency of receiving solar energy is relatively low [2, 3]. Although the efficiency of receiving solar energy is 5%~10% higher than that of a single axis, the dual-axis tracking mechanism has the disadvantages of a large load, obvious accumulated error and high maintenance cost [4, 5]. To solve these problems, researchers began to focus on novel

tracking mechanisms. Wu *et al.* [6] proposed a 2-degree of freedom (DOF) U-3PSS parallel mechanism as the sun tracking mechanism, in which the tracking mechanism's stiffness and the moving platform's rotation ability have increased, but it is not easy to control. Du *et al.* [7] designed a sun tracking mechanism based on the U-PRU-PUS parallel mechanism, which has high structural stiffness and decoupling characteristics of the motion of the moving platform, but its structure is complex and its stability is difficult to maintain. He *et al.* [8] designed a 3-DOF sun tracking mechanism based on the 3-RPS and then adjusted the position and orientation of the PV panel to track the sun by using three wire ropes, which have poor rigidity and small load capacity and are vulnerable to wind loads. Dong [9] designed a 2-DOF 3-RPS for a PV tracking system, in which one prismatic joint of the 3-RPS has been fixed, making the number of prismatic joints of the 3-RPS only two so that only two drives need to be provided, which can reduce energy consumption. However, the motion space of the tracking mechanism will decrease, and solar tracking cannot be carried out over a large range, which reduces the solar energy utilization rate. Shyam *et al.* [10, 11] proposed a 3-DOF 3-RPS to track the sun in a central receiver tower based on a concentrated solar power system. The cone angle of the spherical joints used in the 3-RPS prototype is approximately $\pm 32^\circ$. Therefore, the motion of the 3-RPS heliostat prototype is limited by the rotation angle of the spherical joints. The experimental results also show that actual sun tracking is carried out only from 11:15 am to 3:30 pm. Zheng *et al.* [12, 13] proposed an ultralight dish solar convergence tracking system based on 3-RPS, where the spherical joint is designed as a composite hinge composed of a hook hinge and a rotary hinge. Compared with general form 3-RPS, although the motion space of the new type 3-RPS has increased, the forces on the composite hinge are unreasonable and not easy to keep balance, and the rigidity and the support ability of the tracking mechanism also become lower.

According to previous research, the parallel mechanism has great application potential in solar tracking due to the advantages of independent drive, high stiffness and no cumulative error. Among them, the 3-RPS has the simplest structure and only includes three linear actuators. When it is used as a solar tracking mechanism, it can not only save materials and energy but also be easy to control. However, the application of the general 3-RPS is limited due to the small moving space of the spherical joint and the insufficient support capacity. Therefore, in this paper, the traditional spherical joint of 3-RPS is improved to a passive composite spherical joint, which increases the stiffness of the spherical joint and the range of motion of the output rod. Secondly, each improved 3-RPS is used to drive the reflective mirror facet (not the parabolic dish concentrator) to move cooperatively so that the normal line of the dish concentrator is parallel to the incident sunlight to realize solar tracking. Compared with the existing dish solar tracking mechanism, the novel dish solar tracking system has the advantages of high rigidity of the driving mechanism and large load capacity, the facet shape of the concentrator is not easily deformed by wind load and the size of the concentrator can be flexibly expanded (realized by changing the number of N). Finally, based on the proposed novel dish solar tracking mechanism, we have carried out research on the establishment of the kinematics model of the 3-RPS associated with the solar altitude and azimuth angles, the optimization of the centroid height of the concentrator with genetic algorithm (GA) to solve the problem of too many telescopic rods of the 3-RPS and using particle swarm optimization (PSO) to tune PID parameters for solar trajectory tracking in the visual simulation platform.

2. The working principle of the novel parabolic dish solar tracking platform

The novel dish solar tracking platform proposed in this paper is mainly composed of N improved 3-RPSs, parabolic reflective mirror facets, mounting brackets and a solar heat receiver, in which each reflective mirror facet is mounted on the moving platform of the 3-RPS, and the structure diagram when $N = 4$ is shown in Fig. 1. After the prismatic of these 3-RPSs are driven, the lengths of the telescopic rods can be changed to make the moving platform move so that the reflective mirror facets installed on the moving platforms move together.

The 3-RPS is a symmetrical 3-DOF parallel mechanism that can realize 2-DOF rotation and 1-DOF movement, composed of a fixed base, a moving platform and three identical RPS telescopic rods. The

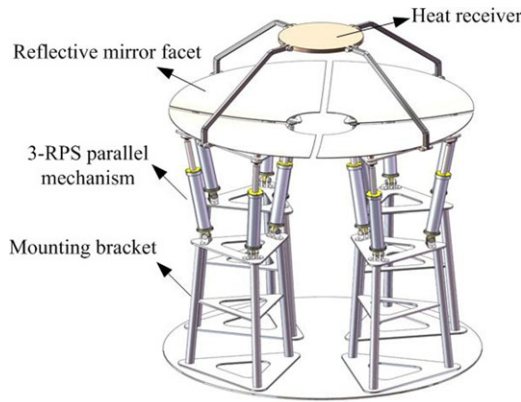


Figure 1. Structure of the novel parabolic dish solar tracking platform.

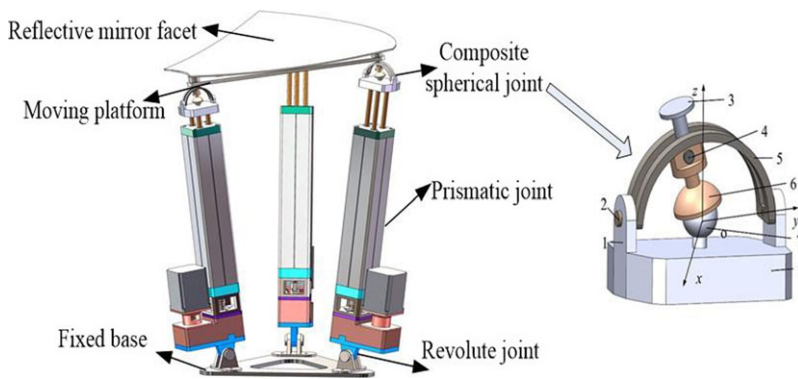


Figure 2. Structure diagram of the 3-RPS parallel tracking mechanism. 1. Binaural support; 2. pin; 3. output rod; 4. support roller; 5. U-shaped shift fork; 6. ball socket; 7. base.

revolute joints (R-joints) and the spherical joints (S-joints) are attached to the fixed base and the moving platform, respectively. The telescopic rod lengths are adjustable by prismatic joints (P-joints), generating a coupled 3-DOF motion of the moving platform.

For the general form 3-RPS, the rotation range of the P-joint is only $-32^{\circ} \sim 32^{\circ}$ due to the limitation of the geometric structure, which makes it challenging to meet the design requirements of the solar tracking platform [14]. In this paper, the bionic passive spherical joint is improved to be the passive composite spherical joint for the 3-RPS of the novel dish solar tracking platform, in which the ball socket and ball head are adjusted so that the rotation range of the new passive joint can reach $-59^{\circ} \sim 59^{\circ}$. The detailed design process can be found in the authors' previous research work [15]. The structure diagram of the 3-RPS solar tracking mechanism is shown in Fig. 2.

3. The coordinate system and coordinate transformation

3.1. The coordinate systems for the novel dish solar tracking platform

The schematic diagram of the coordinate systems of the novel dish solar tracking platform is shown in Fig. 3. Points P and M are the centroids of the 3-RPS fixed base and moving platform, respectively. Point O is the centroid of the dish concentrator and its projection on the ground is point H. During sun tracking, the coordinates of points P, O and H are constant and the position of point M changes with the movement of the three telescopic rods of 3-RPS. Take points O, H, M and P as coordinate origins,

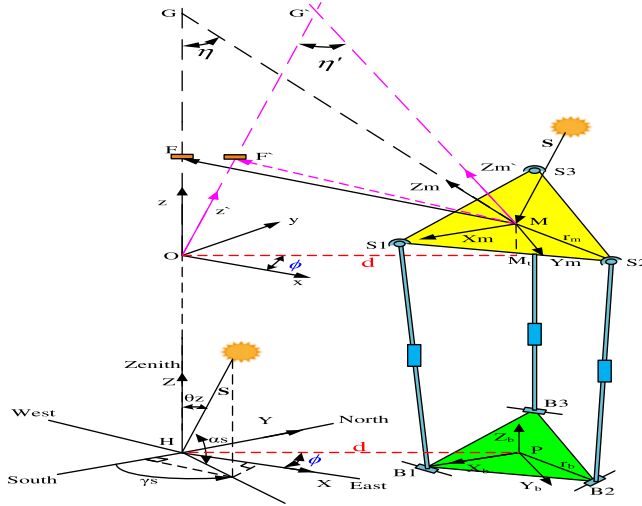


Figure 3. Schematic diagram of the coordinate system for the novel dish solar tracking platform.

then establish the dish coordinate system O-xyz, the horizontal coordinate system H-XYZ, the moving coordinate system M-X_mY_mZ_m and the fixed coordinate system P-X_pY_pZ_p, which will be abbreviated as {O}, {H}, {M}, {P} in this paper. The coordinate axes X, Y and Z point to the east, north and zenith, respectively. The projection of point M on the O-xy plane is M_t. The vertical distances from point P to H and from point M_t to O are equal, which is *d*. The radii of the fixed platform and moving platform of the 3-RPS are *r_b* and *r_m*, respectively. *φ* is the angle between the vector OM_t and the x axis of the coordinate system {O} and is also the angle between the vector HP and the X axis of the coordinate system {H}. *α_s* and *γ_s* are altitude angle and azimuth angle, respectively. Point G and angle *η* are the intersection point and the included angle of the normal line passing through point M and the normal line passing through point O, respectively.

3.2. Coordinate transformation matrix

3.2.1. Rotation transformation matrix from {M} to {O}

Let the coordinates of the origin M of coordinate system {M} in coordinate system {O} be (*x_{m_o}*, *y_{m_o}*, *z_{m_o}*). Since the moving platform of the 3-RPS is on the tangent plane of the rotating paraboloid and point M is the tangent point of the two planes, point M satisfies the rotating paraboloid equation shown in Eq. (1):

$$F(x_{m_o}, y_{m_o}, z_{m_o}) = x_{m_o}^2 + y_{m_o}^2 - 4fz_{m_o} = 0 \tag{1}$$

Then the coordinates of point M in the coordinate system {O} can be written as:

$$M_{-O} = (d \cos \phi, \quad d \sin \phi, \quad (d^2 \cos^2 \phi^2 + d^2 \sin^2 \phi^2) / 4f)^T \tag{2}$$

where *f* is the focal length of the rotating paraboloid dish concentrator, $f = \frac{D(1 + \cos(\theta_{rim}))}{4 \sin(\theta_{rim})}$, *D* and *θ_{rim}* are the diameter and edge angle, respectively.

The equation for the normal line passing through point M can be expressed as:

$$\frac{x - y_{m_o}}{\partial F / \partial x_{m_o}} = \frac{x - y_{m_o}}{\partial F / \partial y_{m_o}} = \frac{z - z_{m_o}}{\partial F / \partial z_{m_o}} \tag{3}$$

where $\partial F/x_{m_o}$, $\partial F/y_{m_o}$ and $\partial F/z_{m_o}$ can be obtained from the partial derivative of Eq. (1) as follows:

$$\left\{ \frac{\partial F}{x_{m_o}} = 2x_{m_o}, \frac{\partial F}{y_{m_o}} = 2y_{m_o}, \frac{\partial F}{z_{m_o}} = -4f \right\} \tag{4}$$

Let the coordinates of point G in coordinate system {O} be $(0, 0, z_{G_o})^T$, then substitute the coordinates of point G into Eq. (4), and the included angle η of the normal line passing through point M and the normal line passing through point O can be obtained by combining Eqs. (4)–(7).

$$|\vec{GO}| = \sqrt{(-z_{G_o})^2} \tag{5}$$

$$|\vec{GM_o}| = \sqrt{(x_{m_o})^2 + (y_{m_o})^2 + (z_{m_o} - z_{G_o})^2} \tag{6}$$

$$\eta = \arccos \left(\frac{\vec{GO} \cdot \vec{GM}}{|\vec{GO}| \cdot |\vec{GM}|} \right), \quad 0 \leq \eta \leq 90 \tag{7}$$

It can be seen from Fig. 3 that the coordinate system {O} can be obtained by rotating {M} clockwise η around Y_m -axis and clockwise ϕ around Z_m -axis. The homogeneous transformation matrix of frame {M} to frame{O} can be expressed as in Eq. (8):

$${}^oT_M = \begin{bmatrix} {}^oR_M & M_{-o} \\ 0 & 1 \end{bmatrix} = \begin{bmatrix} -\cos \eta \cos \phi & \sin \phi & -\cos \phi \sin \eta & d \cos \phi \\ -\cos \eta \sin \phi & -\cos \phi & -\sin \eta \sin \phi & d \sin \phi \\ -\sin \eta & 0 & \cos \eta & \frac{d^2 \cos^2 \phi + d^2 \sin^2 \phi}{4f} \\ 0 & 0 & 0 & 1 \end{bmatrix} \tag{8}$$

3.2.2. Rotation transformation matrix from {P} to {O}

It can also be seen from Fig. 3 that the coordinate system {P} rotates $(\phi - 180)^\circ$ around the Z axis to obtain coordinate system {H}, and the coordinates of point P in the coordinate system {H} are $(d \cos \phi, d \sin \phi, 0)^T$. Then, the rotation transformation matrix of coordinate system {P} with respect to coordinate system {H} can be expressed as:

$${}^HT_P = \begin{bmatrix} {}^HR_P & P_{-H} \\ 0 & 1 \end{bmatrix} = \begin{bmatrix} -\cos \phi & \sin \phi & 0 & d \cos \phi \\ -\sin \phi & -\cos \phi & 0 & d \sin \phi \\ 0 & 0 & 1 & 0 \\ 0 & 0 & 0 & 1 \end{bmatrix} \tag{9}$$

3.2.3. The transformation matrix of the dish concentrator with respect to {H}

For solar tracking, the attitude of the dish concentrator is known, and only the length of the three telescopic rods of the 3-RPS needs to be determined. To obtain the analytical relationship between the length of the telescopic rod, the solar altitude angle and the solar azimuth angle, the attitude of the dish parabolic concentrator can be described as follows:

$$\Phi_{dish} = (x_{O_H}, y_{O_H}, z_{O_H}, \alpha, \beta, \gamma) \tag{10}$$

where x_{O_H} , y_{O_H} and z_{O_H} are the coordinates of the mass center of the parabolic dish concentrator in the coordinate system {H}. α , β and γ are the Euler angles in the form of ZYZ, which are used to describe the attitude of the dish concentrator with respect to coordinate system {H}, and the corresponding homogeneous transformation matrix is

$${}^H T_O = \begin{bmatrix} \cos\alpha \cos\beta \cos\gamma - \sin\alpha \sin\gamma & -\cos\alpha \cos\beta \sin\gamma - \sin\alpha \cos\gamma & \cos\alpha \sin\beta & x_{O_H} \\ \sin\alpha \cos\beta \cos\gamma + \cos\alpha \sin\gamma & -\sin\alpha \cos\beta \sin\gamma + \cos\alpha \cos\gamma & \sin\alpha \sin\beta & y_{O_H} \\ -\sin\beta \cos\gamma & \sin\beta \sin\gamma & \cos\beta & z_{O_H} \\ 0 & 0 & 0 & 1 \end{bmatrix} \tag{11}$$

Then the attitude transformation matrix of the 3-RPS moving platform with respect to the horizon coordinate system {H} is

$${}^H T_M = \begin{bmatrix} {}^H R_M & M_{-H} \\ 0 & 1 \end{bmatrix} = \begin{bmatrix} n_1 & o_1 & a_1 & x_{m_H} \\ n_2 & o_2 & a_2 & y_{m_H} \\ n_3 & o_3 & a_3 & z_{m_H} \\ 0 & 0 & 0 & 1 \end{bmatrix} \tag{12}$$

where $M_{-H} = (x_{m_H}, y_{m_H}, z_{m_H})^T$ describes the position of the origin of the coordinate system {M} and orientation vectors $n = (n_1, n_2, n_3)^T$, $o = (o_1, o_2, o_3)^T$, $a = (a_1, a_2, a_3)^T$ are the directional cosines of the axes X_m, Y_m, Z_m with respect to the coordinate system {H}. From the algorithm of continuous transformation of the rigid body relative to the coordinate system, the following equation can be obtained.

$${}^H T_M = {}^H T_O {}^O T_M \tag{13}$$

Then combine Eq. (8) and Eqs. (11)–(13) to obtain the elements of the ${}^H T_M$ matrix as follows:

$$\begin{aligned} n_1 &= \cos\eta \cos\phi (\sin\alpha \sin\gamma - \cos\alpha \cos\beta \cos\gamma) + \cos\eta \sin\phi (\cos\gamma \sin\alpha + \cos\alpha \cos\beta \sin\gamma) \\ &\quad - \cos\alpha \sin\beta \sin\eta \\ n_2 &= -\cos\eta \cos\phi (\cos\alpha \sin\gamma + \cos\beta \cos\gamma \sin\alpha) - \cos\eta \sin\phi (\cos\alpha \cos\gamma - \cos\beta \sin\alpha \sin\gamma) \\ &\quad - \sin\alpha \sin\beta \sin\eta \\ n_3 &= \sin\beta \cos\eta \cos\gamma \cos\phi - \cos\beta \sin\eta - \sin\beta \cos\eta \sin\gamma \sin\phi \\ o_1 &= \cos\phi (\cos\gamma \sin\alpha + \cos\alpha \cos\beta \sin\gamma) - \sin\phi (\sin\alpha \sin\gamma - \cos\alpha \cos\beta \cos\gamma) \\ o_2 &= \sin\phi (\cos\alpha \sin\gamma + \cos\beta \cos\gamma \sin\alpha) - \cos\phi (\cos\alpha \cos\gamma - \cos\beta \sin\alpha \sin\gamma) \\ o_3 &= -\sin\eta \sin\phi (\cos\alpha \cos\gamma - \cos\beta \sin\alpha \sin\gamma) - \cos\phi \sin\eta (\cos\alpha \sin\gamma + \cos\beta \cos\gamma \sin\alpha) \\ &\quad + \cos\eta \sin\alpha \sin\beta \\ a_1 &= \cos\phi \sin\eta (\sin\alpha \sin\gamma - \cos\alpha \cos\beta \cos\gamma) + \sin\eta \sin\phi (\cos\gamma \sin\alpha + \cos\alpha \cos\beta \sin\gamma) \\ &\quad + \cos\alpha \cos\eta \sin\beta \\ a_2 &= -\sin\eta \sin\phi (\cos\alpha \cos\gamma - \cos\beta \sin\alpha \sin\gamma) - \cos\phi \sin\eta (\cos\alpha \sin\gamma + \cos\beta \cos\gamma \sin\alpha) \\ &\quad + \cos\eta \sin\alpha \sin\beta \\ a_3 &= \cos(\beta) \cos(\eta) + \cos(\gamma) \cos(\phi) \sin(\beta) \sin(\eta) - \sin(\beta) \sin(\eta) \sin(\gamma) \sin(\phi) \\ x_{m-H} &= \cos\alpha \sin\beta (d^2 \cos^2\phi + d^2 \sin^2\phi) / (4f) - d \sin\phi (\cos\gamma \sin\alpha + \cos\alpha \cos\beta \sin\gamma) \\ &\quad - d \cos\phi (\sin\alpha \sin\gamma - \cos\alpha \cos\beta \cos\gamma) \\ y_{m-H} &= \sin\alpha \sin\beta (d^2 \cos^2\phi + d^2 \sin^2\phi) / (4f) + d \cos\phi (\cos\alpha \sin\gamma + \cos\beta \cos\gamma \sin\alpha) \\ &\quad + d \sin\phi (\cos\alpha \cos\gamma - \cos\beta \sin\alpha \sin\gamma) \\ z_{m-H} &= z_{o-H} + \cos\beta (d^2 \cos^2\phi + d^2 \sin^2\phi) / (4f) - d \cos\gamma \cos\phi \sin\beta + d \sin\beta \sin\gamma \sin\phi \end{aligned}$$

The movement of the 3-RPS moving platform is constrained by spherical joints, so its three legs can only move in the planes of $y_{S_1-H} = 0, y_{S_2-H} = -\sqrt{3}x$ and $y_{S_3-H} = \sqrt{3}x_{S_3-H}$. Then the constraint relations of

x_{m-H} and y_{m-H} are obtained as follows:

$$x_{m-H} = -0.5r_m \begin{pmatrix} \cos \eta \cos \phi (\cos \alpha^2 \cos \beta - \cos \alpha^2 + 1) + 0.5 \sin 2\alpha \cos \eta \sin \phi (\cos \beta - 1) \\ -\cos \phi (\cos \alpha^2 + \cos \beta \sin \alpha^2) + 0.5 \sin 2\alpha \sin \phi (\cos \beta - 1) + \cos \alpha \sin \beta \sin \eta \end{pmatrix} \quad (14)$$

$$y_{m-H} = r_m (\cos \eta \sin \phi (\cos \alpha^2 + \cos \beta \sin \alpha^2) + \cos \alpha \cos \eta \cos \phi \sin \alpha (\cos \beta - 1) + \sin \alpha \sin \beta \sin \eta) \quad (15)$$

As shown in Fig. 3, since the parabolic dish concentrator cannot rotate around the Z axis and the path of the sun in a day is basically symmetrical with respect to the ZHX plane, the relationship between the Euler angle, altitude angle α_s and azimuth angle γ_s is obtained

$$\begin{cases} \alpha = 90 - \gamma_s \\ \beta = 90 - \alpha_s \\ \gamma = -\alpha \end{cases} \quad (16)$$

4. Inverse kinematics of the 3-RPS parallel manipulator

4.1. Length of the 3-RPS telescopic rod

According to the geometric shape of the 3-RPS, the coordinates of the rotary joints in coordinate system {P} are given by $\overrightarrow{PB_1} = (r_b, 0, 0)^T$, $\overrightarrow{PB_2} = (-\frac{1}{2}r_b, \frac{\sqrt{3}}{2}r_b, 0)^T$ and $\overrightarrow{PB_3} = (-\frac{1}{2}r_b, -\frac{\sqrt{3}}{2}r_b, 0)^T$. The coordinates of the spherical joints in coordinate system {M} are given by $\overrightarrow{MS_1} = (r_m, 0, 0)^T$, $\overrightarrow{MS_2} = (-\frac{1}{2}r_m, \frac{\sqrt{3}}{2}r_m, 0)^T$ and $\overrightarrow{MS_3} = (-\frac{1}{2}r_m, -\frac{\sqrt{3}}{2}r_m, 0)^T$. It can be seen from Eq. (9) and Eqs. (12)–(15), ${}^H T_P$ is determined by parameters ϕ and d , and ${}^H T_M$ is determined by parameters $z_{o-H}, \alpha_s, \gamma_s, \eta, \phi, r_m$ and d . In order to express the relationship more clearly, ${}^H T_P$ and ${}^H T_M$ can be written as ${}^H T_P(\phi, d)$ and ${}^H T_M(z_{o-H}, \alpha_s, \gamma_s, \eta, \phi, r_m, d)$. Then the position vector of the spherical joints S_i ($i = 1, 2, 3$) with respect to the coordinate system {H} is given as

$$\begin{bmatrix} \overrightarrow{B_i S_i} \\ 1 \end{bmatrix} = {}^H T_M(z_{o-H}, \alpha_s, \gamma_s, \eta, \phi, r_m, d) \begin{bmatrix} \overrightarrow{M S_i} \\ 1 \end{bmatrix} - {}^H T_P(\phi, d) \begin{bmatrix} \overrightarrow{P B_i} \\ 1 \end{bmatrix} \quad (17)$$

Then the length l_i ($i = 1, 2, 3$) of each telescopic rod of the 3-RPS can be written as:

$$l_i = \left\| \overrightarrow{B_i S_i} \right\| \quad (18)$$

According to the comprehensive analysis of Eqs. (17)–(18), the telescopic rod lengths of the 3-RPS in this novel dish concentrator platform are mainly determined by the parameters $z_{o-H}, \alpha_s, \beta_s, \phi, \eta, r_m, r_b$ and d . But the parameters ϕ, η, r_m, r_b and d are related to the structure sizes and installation position of the 3-RPS and the parabolic dish concentrator. Therefore, only the three parameters of α_s, β_s and z_{o-H} are needed after the sizes and installation position are known, and solar tracking can be realized. The position and orientation of the 3-RPS moving platform can be written as:

$$W_{3-RPS} = \Phi(\alpha_s, \gamma_s, z_{o-H}) \quad (19)$$

4.2. The velocity of the 3-RPS manipulator

${}^H V_M$ is the linear velocity of the center point of the moving platform; ${}^H \omega_M$ is the angular velocity of the moving platform; ${}^H r_{S_i}$ is the radius vector from the spherical joint S_i to point M; ${}^H V_{S_i}$ is the velocity of the spherical joint S_i ; L_i is the length vector of the telescopic rod and ${}^H e_i$ is the unit vector of L_i where ${}^H e_i = L_i/l_i$, and \dot{l}_i is the drive velocity of L_i .

The velocity vector of spherical joint S_i can be written as:

$${}^H V_{S_i} = {}^H V_M + {}^H \omega_M \times {}^H r_{S_i} \tag{20}$$

The driving velocity \dot{l}_i can be expressed as the projection of ${}^H V_{S_i}$ on L_i .

$$\dot{l}_i = {}^H V_{S_i} \cdot {}^H e_i = \begin{bmatrix} {}^H e_i^T ({}^H r_{S_i} \times {}^H e_i)^T \\ {}^H V_M \end{bmatrix} \tag{21}$$

The length vector of the three telescopic rods of the 3-RPS is

$$\dot{L}_i = J_A \begin{bmatrix} {}^H V_M \\ {}^H \omega_M \end{bmatrix} \tag{22}$$

where $\dot{L}_i = [\dot{l}_1, \dot{l}_2, \dot{l}_3]^T, J_A = \begin{bmatrix} {}^H e_1^T & ({}^H r_{S1} \times {}^H e_1)^T \\ {}^H e_2^T & ({}^H r_{S2} \times {}^H e_2)^T \\ {}^H e_3^T & ({}^H r_{S3} \times {}^H e_3)^T \end{bmatrix}_{3 \times 6}$

Derive from Eqs. (14)–(15) to obtain the linear velocity of the 3-RPS moving platform as follows:

$${}^H V_M = J_v \begin{bmatrix} \dot{\alpha} \\ \dot{\beta} \\ \dot{Z}_{-H} \end{bmatrix} = [Jv1, Jv2, Jv3] \begin{bmatrix} \dot{\alpha} \\ \dot{\beta} \\ \dot{Z}_{-H} \end{bmatrix} \tag{23}$$

where

$$J_{v1} = \begin{bmatrix} 0.5r_m \begin{pmatrix} (\cos \beta - 1) \cos \phi \sin 2\alpha + \sin \eta \sin \alpha \sin \beta \\ -(\cos \beta - 1)(k_2 + \sin \phi) \cos 2\alpha + k_1(\cos \beta - 1) \sin 2\alpha \end{pmatrix} \\ r_m \begin{pmatrix} k_1(\cos \beta - 1) \cos \alpha^2 + \sin \eta \sin \beta \cos \alpha \\ + 2k_2(\cos \beta - 1) \cos \alpha \sin \alpha - k_1(\cos \beta - 1) \sin \alpha^2 \\ 0 \end{pmatrix} \end{bmatrix}$$

$$J_{v2} = \begin{bmatrix} 0.5r_m (\sin \beta \cos \alpha^2 k_4 + k_1 \sin 2\alpha \sin \beta - \sin \eta \cos \alpha \cos \beta - \cos \phi \sin \beta) \\ -r_m \sin \alpha (k_1 \cos \alpha \sin \beta - \sin \eta \cos \beta + k_2 \sin \alpha \sin \beta) \\ 0 \end{bmatrix}$$

$$J_{v3} = [0 \ 0 \ 1]^T$$

$$k_1 = \cos \eta \cos \phi, k_2 = \sin \phi \cos \eta, k_3 = 0.5 \sin \phi (\cos \eta + 1), k_4 = k_1 + \cos \phi.$$

The relationship between the angular velocity of the 3-RPS moving platform and the rotation matrix is as follows:

$${}^H \omega \times = {}^H \dot{R}_M^H R_M^{-1} = \begin{bmatrix} 0 & -{}^H \omega_z & {}^H \omega_y \\ {}^H \omega_z & 0 & -{}^H \omega_x \\ -{}^H \omega_y & {}^H \omega_x & 0 \end{bmatrix} \tag{24}$$

The angular velocity of the 3-RPS moving platform is obtained by combining Eq. (12) and Eq. (24) as follows:

$${}^H \omega_M = \begin{bmatrix} 0 & -\sin \alpha & \sin \beta \cos \alpha \\ 0 & \cos \alpha & \sin \beta \sin \alpha \\ 1 & 0 & \cos \beta \end{bmatrix} \begin{bmatrix} \dot{\alpha} \\ \dot{\beta} \\ -\dot{\alpha} \end{bmatrix} \tag{25}$$

Combining Eq. (23) and Eq. (25) to obtain the velocity of the center of mass of the 3-RPS moving platform.

$$\begin{bmatrix} {}^H V_M \\ {}^H \omega_M \end{bmatrix} = J_B \begin{bmatrix} \dot{\alpha} \\ \dot{\beta} \\ \dot{z}_{O-H} \end{bmatrix} \tag{26}$$

By combining Eq. (22) and Eq. (26), the driving speed \dot{L}_i of the rod can be obtained.

$$\dot{L}_i = J_A J_B \begin{bmatrix} \dot{\alpha} \\ \dot{\beta} \\ z_{O-H} \end{bmatrix} \tag{27}$$

5. Trajectory planning

5.1. Sun position calculation

In order to track the sun in real time, it is necessary to know the solar altitude angle α_s and the solar azimuth angle γ_s , which can be obtained by combining Eq. (28) and Eq. (29) [14, 15]:

$$\alpha_s = \arcsin(\sin L_{at} \sin \delta + \cos L_{at} \cos \delta \cos \omega_s) \tag{28}$$

$$\gamma_s = \text{sgn}\omega_s \cdot \arccos\left(\frac{\sin \alpha_s \sin L_{at} - \sin \delta}{\cos \alpha_s \cos L_{at}}\right) \tag{29}$$

where L_{at} is the local latitude, δ is the sun declination angle, ω_s is the solar hour angle ($\omega_s < 0$ in the morning, $\omega_s = 0$ at noon and $\omega_s > 0$ in the afternoon), $\text{sgn}\omega_s$ is a sign function (when $\omega_s < 0$, $\text{sgn}\omega_s = -1$; when $\omega_s = 0$, $\text{sgn}\omega_s = 0$; when $\omega_s > 0$, $\text{sgn}\omega_s = 1$), δ and ω_s can be determined by Eq. (30) and Eq. (31) [16] [17]:

$$\delta = \frac{180}{\pi} \begin{pmatrix} 0.00148 \sin 3\lambda - 0.399912 \cos \lambda \\ +0.070257 \sin \lambda - 0.006758 \cos 2\lambda \\ +0.000907 \sin 2\lambda - 0.002679 \cos 3\lambda \\ +0.006918 \end{pmatrix} \tag{30}$$

$$\omega_s = 15 \times (S_t - 12) \tag{31}$$

where $\lambda = \frac{360(n-1)}{365}$, n is the product day in the order of days, that is, on January 1, $n = 1$, on January 2, $n = 2, \dots$, until December 31, $n = 365$ (in the common year) or 366 (in the leap year).

$$S_t = S_m + E_t \tag{32}$$

$$S_m = (S_l + F_1/60) - \frac{4}{60} \left(120 - \left(L_o + \frac{F_2}{60} \right) \right) \tag{33}$$

$$E_t = \frac{180}{\pi} \cdot 4 \begin{pmatrix} +0.001868 \cos \lambda - 0.032077 \sin \lambda \\ -0.014615 \cos 2\lambda - 0.0409 \sin 2\lambda \\ +0.000075 \end{pmatrix} \tag{34}$$

where S_t is the hourly value at the observation time; F_1 is the minute value of time; L_o is the degree value of the longitude of the observation location, which is positive in the east longitude and negative in the west longitude; and F_2 is the minute value of longitude.

The extreme values of the inclination angles of the Earth’s rotation axis relative to the sun’s incident light occur at the spring equinox, summer solstice, autumn equinox and winter solstice. Taking Hunan University of Science and Technology (27.9° N, 112.9° E) as the observation point, the trajectories of α_s and γ_s from 9 am to 16 pm on these four special days are shown in Fig. 4, which shows that the change law of α_s in a day increases gradually in the morning, reaches its peak at noon and decreases in the afternoon, and α_s reaches the maximum and minimum values on the summer solstice and the winter solstice, respectively, and α_s at the spring equinox and autumn equinox is nearly equal. The variation of γ_s in a day presents a monotonic decreasing trend and reaches the maximum and minimum values on the summer solstice and the winter solstice, respectively, while the values at the spring and autumn equinoxes are almost equal. In this paper, the trajectories of α_s and γ_s on these four special days will be taken as the inputs of the 3-RPS prismatic joints.

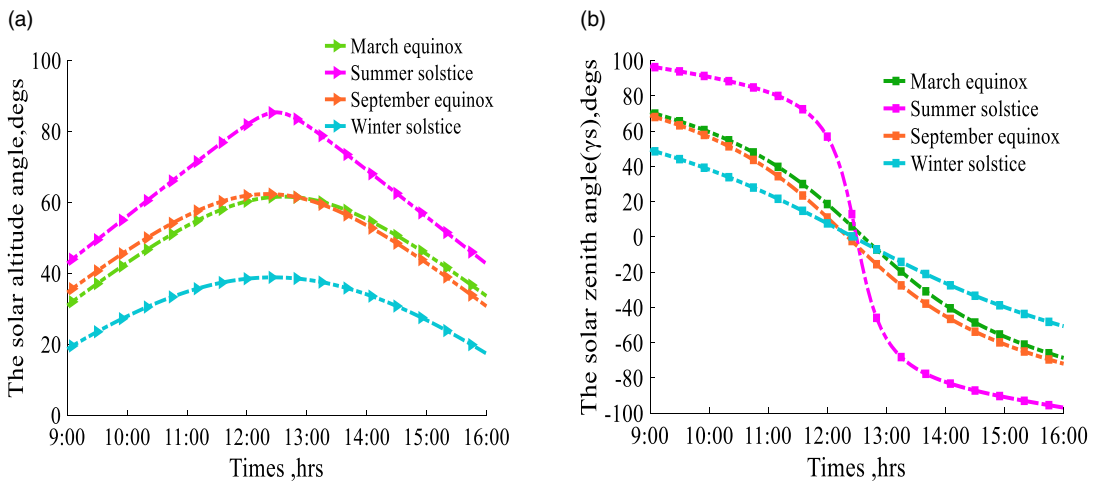


Figure 4. The curve of the solar altitude and azimuth angles. (a) Solar altitude angle. (b) Solar zenith angle.

5.2. Trajectory planning of the 3-RPS parallel manipulator

The structural parameters of the proposed novel dish solar tracking platform are shown in Table 1. The fixed base centroids of the four 3-RPSs are located in the axis +X, +Y, -X and -Y directions of the horizontal coordinate system {H}, namely $\phi = 90(N - 1)$, $N = 1, 2, 3, 4$.

According to the inverse solution formula of 3-RPS, the height of the center of mass (z_{O-H}) of the dish concentrator will affect the length of the telescopic rod of 3-RPS. When the value of z_{O-H} is not taken

Table 1. Structural parameters of the dish solar tracking platform.

Parameters	Values
Diameter of the parabolic dish concentrator, $D/(mm)$	3200
Edge angle of the parabolic dish concentrator, $\theta_{rim}/(^{\circ})$	45
Circumradius of the fixed base of the 3-RPS, $r_b/(mm)$	200
Circumradius of the moving platform of the 3-RPS, $r_m/(mm)$	300
Maximum telescopic rod length of the 3-RPS, $L_{i\max}/(mm)$	4000
Minimum telescopic rod length of the 3-RPS, $L_{i\min}/(mm)$	2000
The vertical distance from point p to H or point M_i to O, $d/(mm)$	800

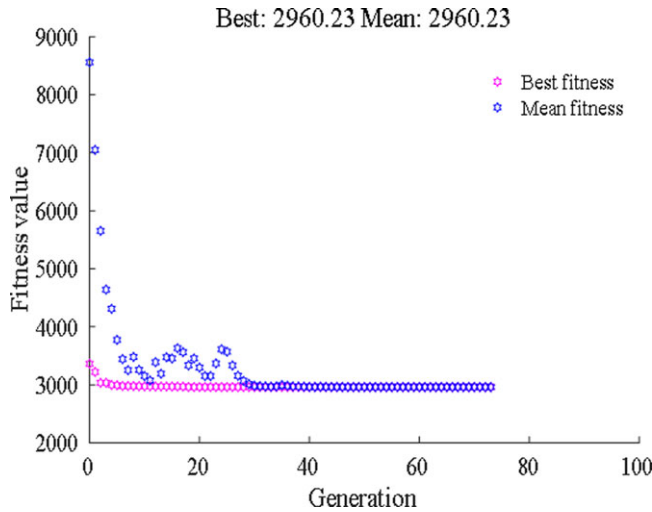


Figure 5. Results of z_{O-H} optimization by GA.

correctly, the number of telescopic rods will reach three or more, making the telescopic rod structure more complex and difficult to control. Therefore, z_{O-H} needs to be optimized to meet the requirements of two telescopic rods. By transforming the 3-RPS inverse solution formula, the optimized objective function and constraints are obtained as shown in formula (35):

$$z_{O-H} = \min \sum_{i=1}^3 \lambda_{i,N} f(l_{i,N}, t) \tag{35}$$

$$s.t. \quad 2000 \leq l_{i,N} \leq 4000$$

$$9 \leq t \leq 16$$

where $f(l_{i,N}, t)$ is a function containing two variables $l_{i,N}$ and t , which can be converted from Eq. (17), $l_{i,N}$ represents the length of the i th telescopic rod of the N th 3-RPS; $\lambda_{i,N}$ is the influence weight of the i th link length of the N th 3-RPS, and since the telescopic rods of the 3-RPS are independent of each other, the values of $\lambda_{i,N}$ can be equal.

Take the parameters in Table 1 into formula (35), and optimize z_{O-H} by using the GA optimization toolbox of MATLAB software to obtain the results shown in Fig. 5.

It can be seen from Fig. 5 that when the number of iterations is 75, the best fitness value of z_{O-H} is 2960.23 mm. Taking this result into the 3-RPS inverse solution formula, calculate the length of the 3-RPS telescopic rod in the spring equinox, summer solstice, autumn equinox and winter solstice, and obtain the motion trajectory as shown in Fig. 6. The minimum and maximum lengths of the telescopic rod are 2105 mm and 3864 mm, respectively. Then a 2-section telescopic rod with a length of both the upper rod and the lower rod of 2000 mm can meet the requirements for the movement of the 3-RPS.

5.3. Attitude simulation of 3-RPS parallel manipulators

In order to analyze the movement posture of four 3-RPSs more intuitively, the kinematics attitude of the 3-RPS is simulated by using MATLAB software. Figures 7–10 show the attitudes of the four 3-RPSs at 10 am, 12 noon and 14 pm on the summer solstice.

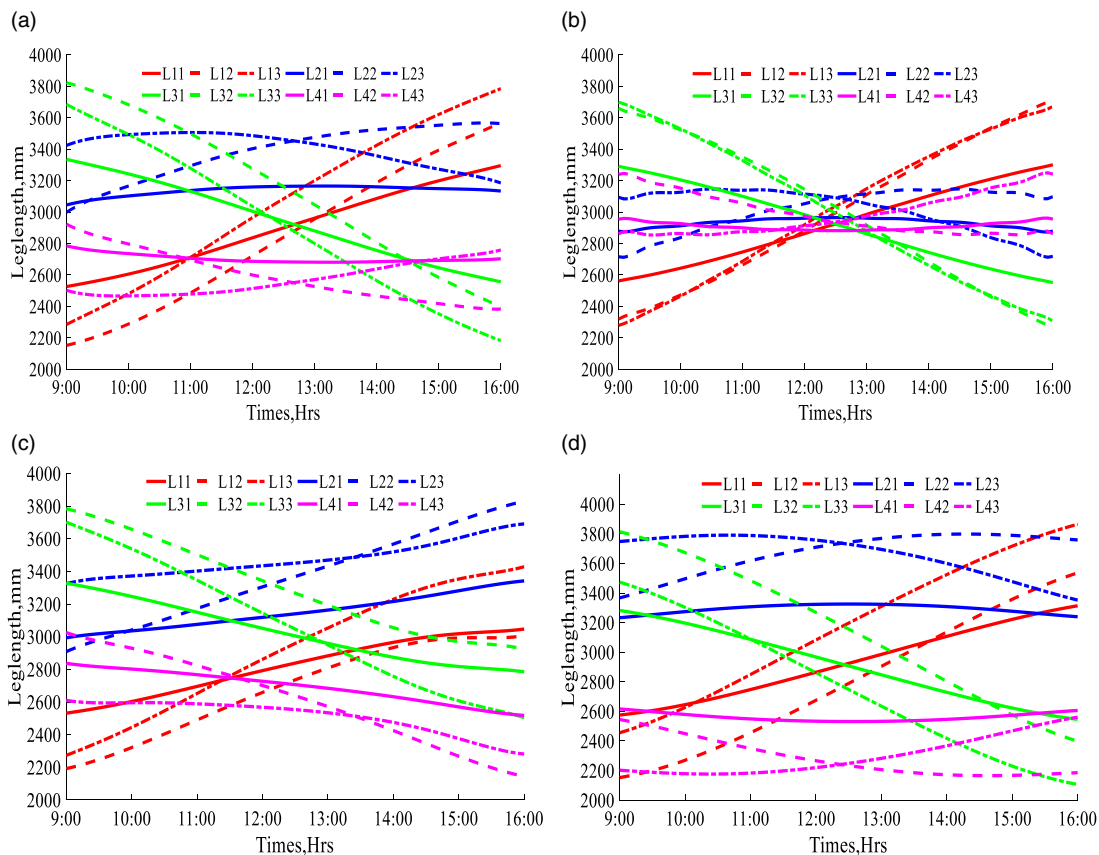


Figure 6. Length of the telescopic rods of the 3-RPS manipulators. (a) March equinox. (b) Summer solstice. (c) September equinox. (d) Winter solstice.

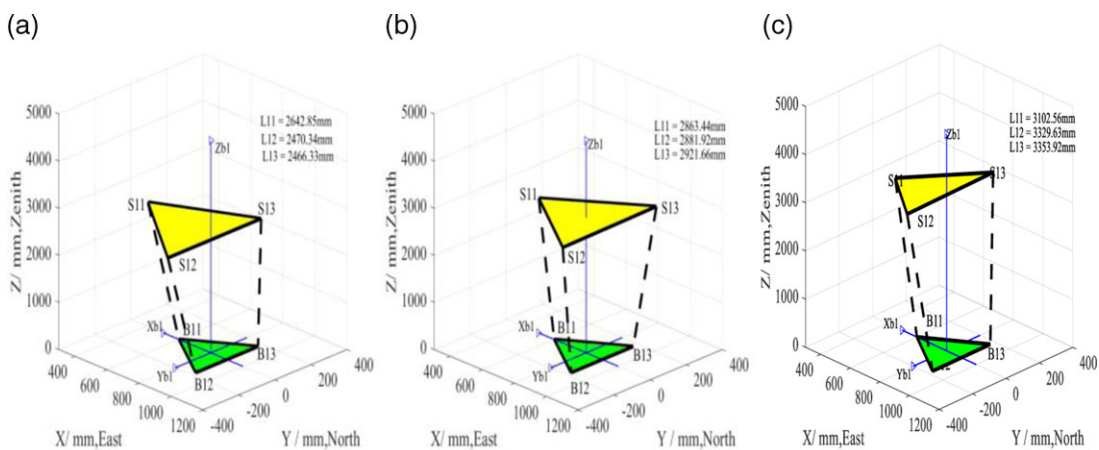


Figure 7. Attitude of the 3-RPS moving platform on the +X axis at the summer solstice. (a) 10:00 am. (b) 12:00 noon. (c) 14:00 pm.

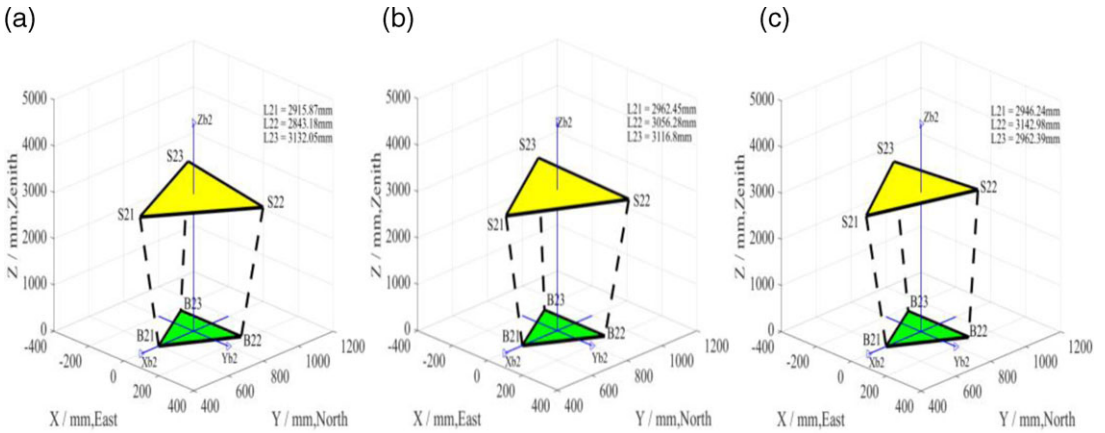


Figure 8. Attitude of the 3-RPS moving platform on the +Y axis at the summer solstice. (a) 10:00 am. (b) 12:00 noon. (c) 14:00 pm.

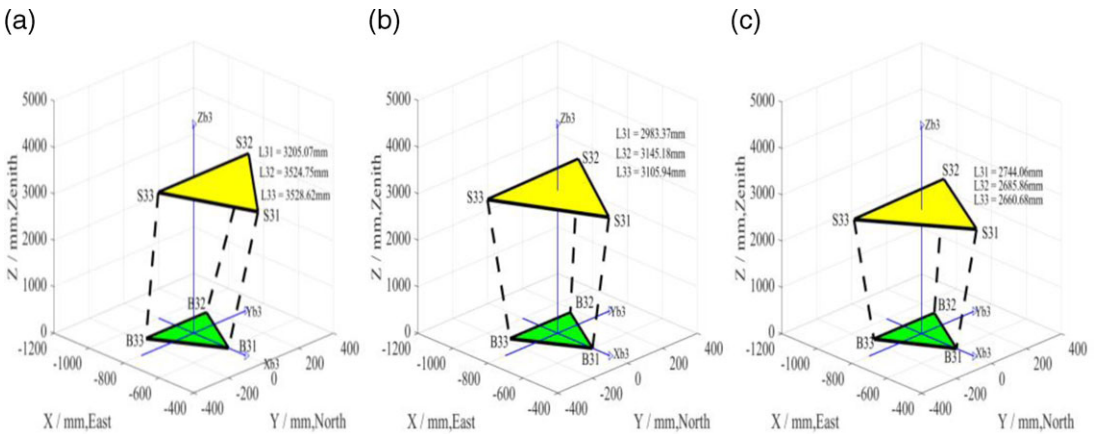


Figure 9. Attitude of the 3-RPS moving platform on the -X axis at the summer solstice. (a) 10:00 am. (b) 12:00 noon. (c) 14:00 pm.

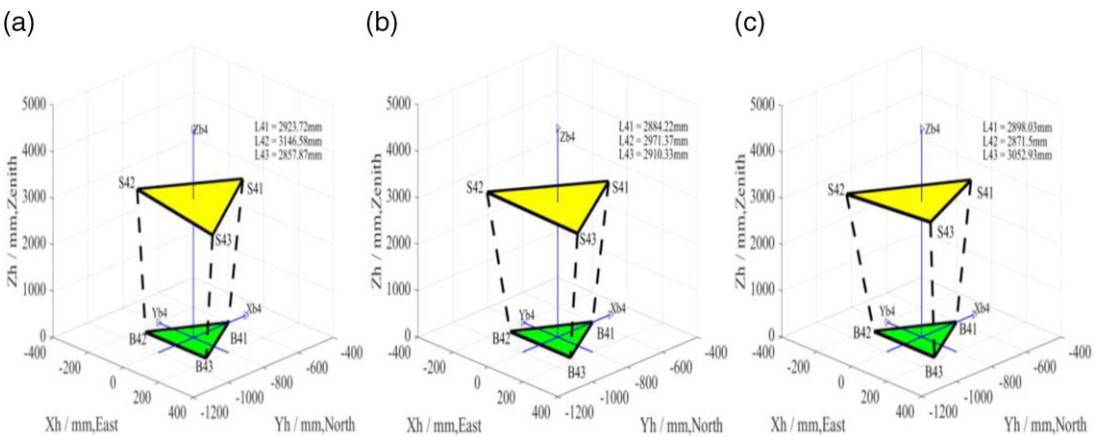


Figure 10. Attitude of the 3-RPS moving platform on the -Y axis at the summer solstice. (a) 10:00 am. (b) 12:00 noon. (c) 14:00 pm.

6. Trajectory tracking and control of the novel dish solar power generation system

6.1. Error evaluation index

To ensure that the 3-RPS can stably and accurately track the sun’s trajectory, the time-weighted integral absolute error (*ITAE*) is used as the performance index of controller design. The expression of *ITAE* index is as follows [18]:

$$J_{ITAE} = \int_0^t t |e(t)| dt \tag{36}$$

The *ITAE* index includes two factors: time and error. It considers the dynamic and steady-state performance of the control system, which can ensure the response speed and steady-state accuracy of the system. The controller of the 3-RPS will be designed with the goal of minimum *ITAE*.

6.2. PID controller

The mathematical expression of the PID controller is

$$u(t) = K_p e(t) + K_i \int_0^t e(\tau) d\tau + K_d \frac{de(t)}{dt} \tag{37}$$

where K_p , K_i and K_d represent the three coefficients of proportion, integral and differential, respectively. The schematic diagram of the PID controller for a single 3-RPS is shown in Fig. 12, where *act_pos*, *des_pos*, *des_el* and *des_vel* are the ideal input position, actual output position, ideal input velocity and actual output velocity for the 3-RPS, respectively, and *force* represents the input driving torque. Since each 3-RPS is in parallel, the PID controller diagrams of the other 3-RPSs are the same as in Fig. 11.

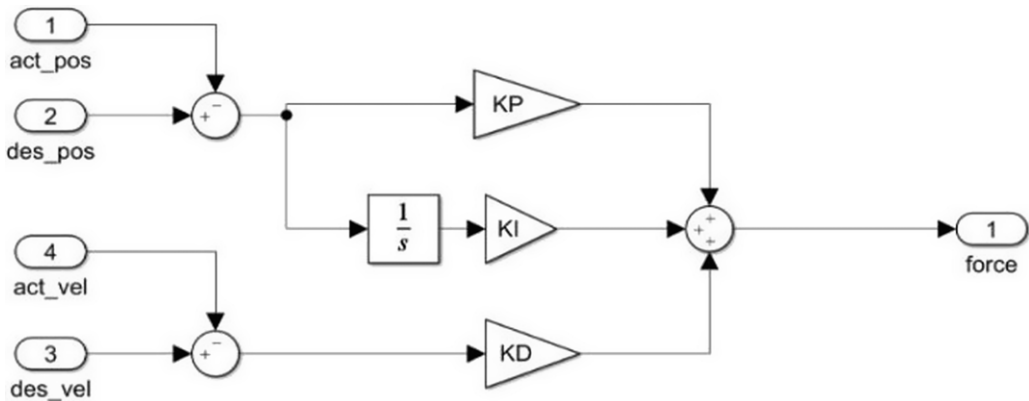


Figure 11. Schematic diagram of the single 3-RPS PID controller.

6.3. PSO-PID controller

PSO is an evolutionary algorithm proposed by J. Kennedy and R. C. Eberhart in 1995. It originates from the migration and clustering behavior of birds in the process of foraging [19]. Its basic idea is to find the optimal solution through cooperation and information sharing among individuals in the group. The update rule of PSO is to initialize a group of random solutions and then find the optimal solution through iteration. In each iteration, the particle updates itself by tracking the extreme individual value P_{best} and the extreme global value G_{best} . After these two optimal values are found, the particle updates its speed and new position through the following formula [20]:

$$v_{t+1} = \omega v_t + c_1 \text{rand} () (p_{rbest} - x_t) + c_2 \text{rand} () (G_{rbest} - x_t) \tag{38}$$

$$x_{t+1} = x_t + v_{t+1} \tag{39}$$

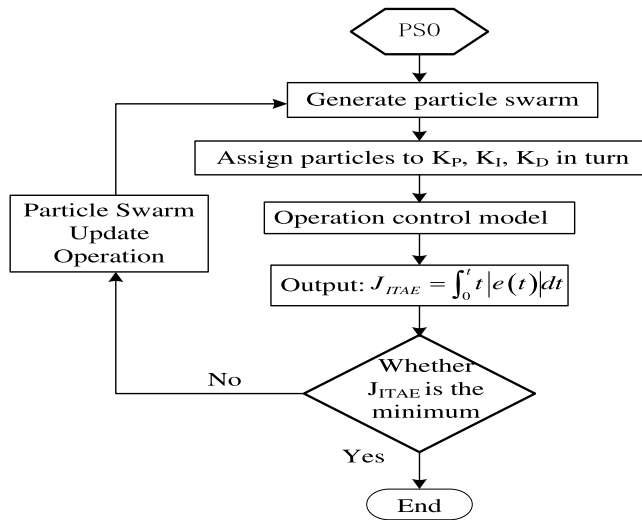


Figure 12. Flow chart of the PID controller optimized by PSO.

where ω is the inertial weight, $t = 1, 2, 3, \dots, T$, and T is the total running time; x_t is the position of the t th particle; v_t is the velocity of the t th particle; p_{tbest} is the optimal position searched by the t th particle; p_{gbest} is the optimal position searched by the whole particle swarm; c_1 and c_2 are learning factors and $\text{rand}()$ is a random number between (0,1). The flow chart of the PID controller optimized by PSO is shown in Fig. 12.

6.4. Trajectory tracking control simulation

A visual simulation model of a rotating parabolic solar power generation system has been established in the Simscape Multibody of MATLAB software, in which driving elements and detection modules were added, and component parameters were set. The control system structure of the visualization platform is shown in Fig. 13, mainly composed of the 3-RPS inverse kinematics models, PSO-PID controller, a multibody physical model of the dish solar tracking platform and the solar trajectory model.

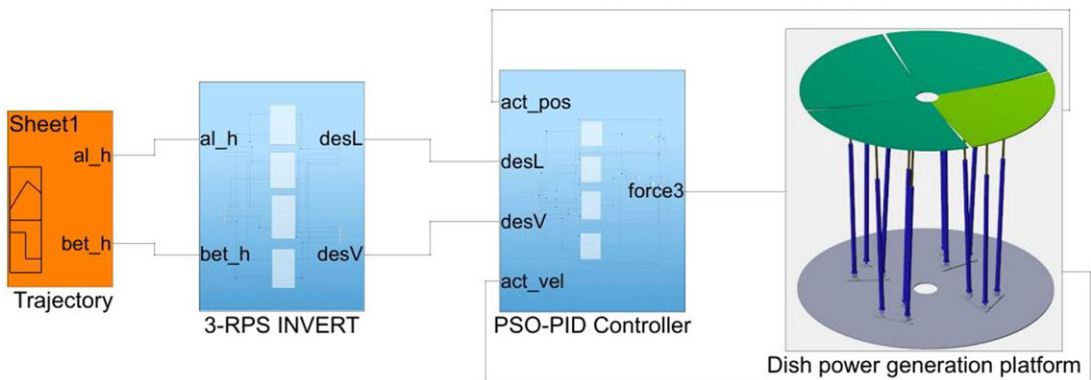


Figure 13. Control schematic diagram of the visual simulation platform.

When the solar altitude angle and the azimuth angle are both 90° , the attitude of the novel dish solar tracking platform is in the initial position. The 3-RPS needs to move from the initial position to the

starting point for tracking before sun tracking in the morning and then move to the initial position after sun tracking in the afternoon. The attitude of the initial position is shown in Fig. 14.

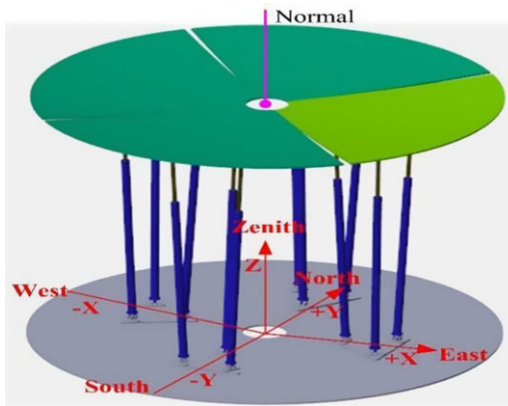


Figure 14. Attitude of the concentrator in the initial position of the novel dish platform.

Based on this visualization platform, the simulation experiment of motion control is carried out by taking the sun tracking on the summer solstice. The PID parameters obtained by PSO are shown in Table 2.

Table 2. Parameters of PSO-PID controller.

Parameters	3-RPS			
	1	2	3	4
K_P	450	600	450	800
K_I	50	60	50	5
K_D	10	15	10	20

The PSO-PID controller is designed by using the PID parameters in Table 2. Experiments are carried out on the visual simulation platform, and the error response of each telescopic rod is shown in Fig. 13 when four 3-RPSs of the dish system track the sun trajectory. Table 3 shows the stability error. It can be seen from Fig. 15 and Table 3 that the PSO-PID controllers on the four 3-RPSs can make the telescopic rod error converge rapidly, which can achieve stable and accurate tracking of the system. In the steady state, the error of the first rod of all 3-RPSs is smaller than that of the other two telescopic rods, mainly because the displacement change of the telescopic rod near the centroid of the concentrator is smaller than the outer layer during the whole tracking work. Figure 16 shows the three attitudes of the

Table 3. Steady-state error.

Error number	3-RPS			
	1	2	3	4
	Er1 (mm)	Er2 (mm)	Er3 (mm)	Er4 (mm)
1	0.95	0.097	0.63	0.0097
2	2.27	0.96	1.29	0.0195
3	2.60	0.36	1.39	0.0375

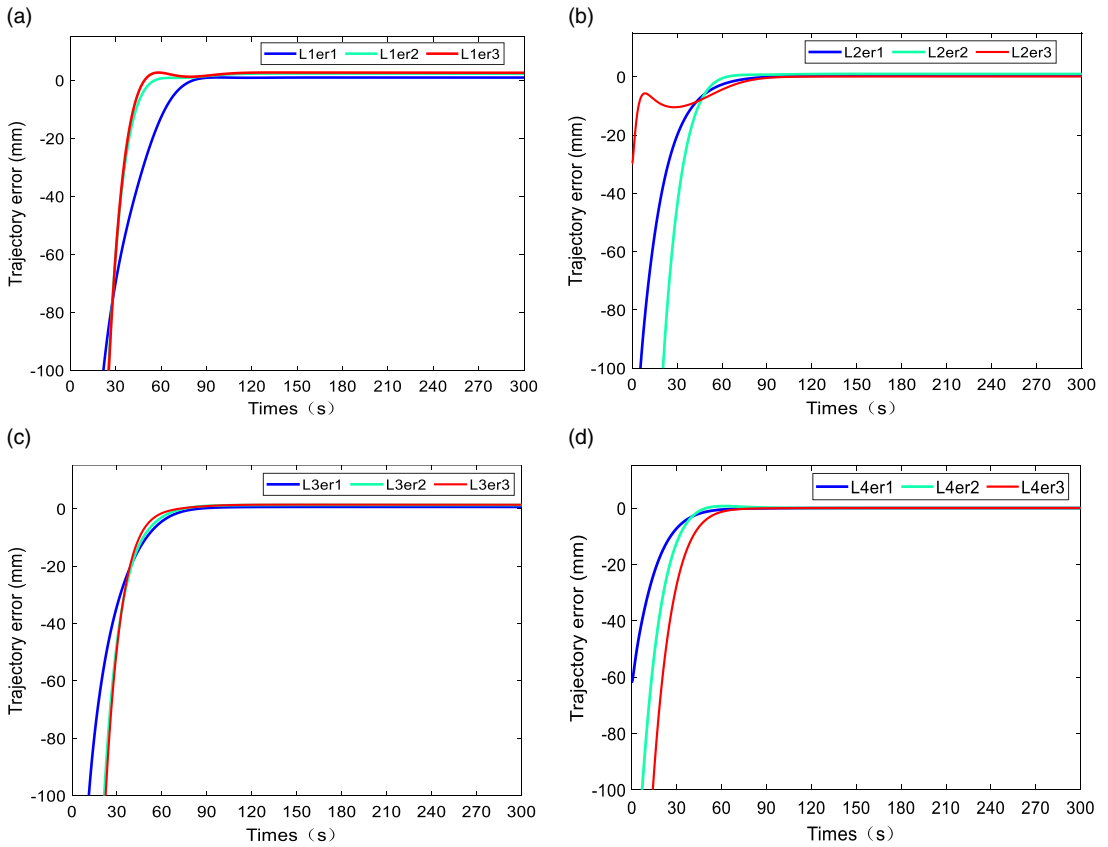


Figure 15. Error response curve of 3-RPS parallel manipulators. (a) Error response curve of 3-RPS on the +X axis. (b) Error response curve of 3-RPS on the +Y axis. (c) Error response curve of 3-RPS on -X axis. (d) Error response curve of 3-RPS on -Y axis.

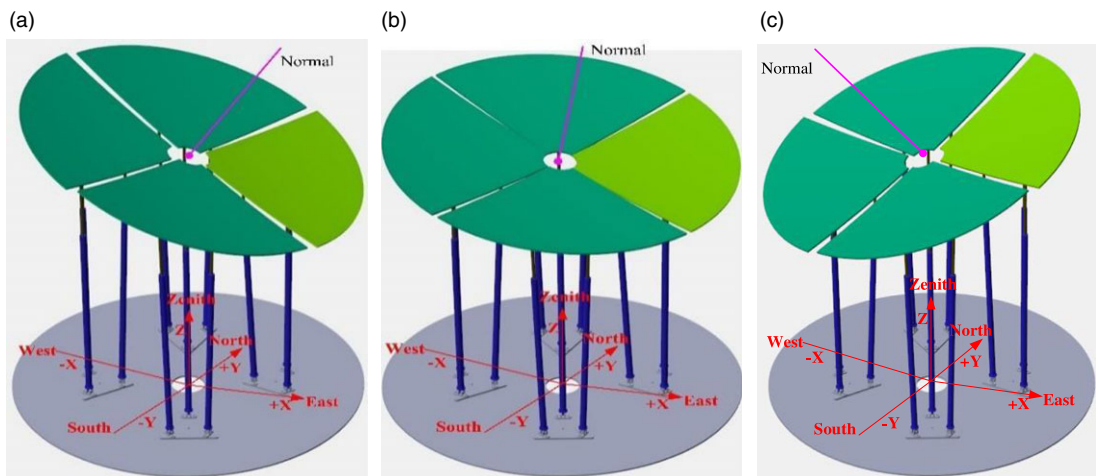


Figure 16. Attitude of the novel dish solar tracking platform on summer solstice. (a) 10:00 am. (b) 12:00 noon. (c) 14:00 pm.

concentrator at 10:00 am, 12:00 noon and 14:00 pm in the visual simulation platform of the novel dish solar power generation system.

7. Conclusions

1. A novel parabolic dish solar concentrator is designed, mainly composed of N 3-RPSs, parabolic reflective mirror facets, mounting brackets and a solar heat receiver. To increase the motion range of the 3-RPS to meet the requirements of dish solar tracking, the spherical joint of the 3-RPS was designed to be a passive composite spherical joint with a limit range of $(-59^\circ \sim 59^\circ)$, which can realize solar trajectory tracking from 9:00 am to 16:00 pm.
2. The kinematics model of the 3-RPS of the novel dish solar concentrator is established, and then the relationships of the displacement and the velocity of the 3-RPS telescopic rod related to the solar altitude and azimuth angles are obtained.
3. Aiming at the problem that the height of the concentrator's center of mass (z_{O-H}) is improperly selected, which causes the number of telescopic rod sections to reach three or more, making the structure of the telescopic rod more complex, z_{O-H} is optimized by GA to be 2960.23 mm, which reduces the number of the sections of the telescopic rod to two, reducing the complexity of the structure and the difficulty of control.
4. The visual simulation platform of the control system is established. To minimize the absolute error of the time-weighted integral, the parameters K_P , K_I and K_D of the PID controller are tuned using the PSO algorithm. Then, taking the summer solstice as an example, the motion control simulation is carried out. The experimental results show that the PSO-PID controller can quickly converge the errors caused by the movement of the telescopic rod, making the sun trajectory tracking errors of these four 3-RPSs within the range of 2.6 mm.

Author contribution. Fanmao Liu and Han Mo conceived the research, Fanmao Liu guided the research and Han Mo carried out theoretical derivation and simulation experiments and wrote this article. Cancan Liao designed the system structure diagram, and Yuanyuan Zhang analyzed the experimental data.

Financial support. This research work was supported by the grants from the General Program of the National Natural Science Foundation of China (No. 51576061) and The Basic Ability Enhancement Program for Young and Middle-aged Teachers of Guangxi, China (No. 2021KY0706).

Competing interests. The authors declare no potential conflicts of interest.

Ethical approval. None.

References

- [1] M. H. Ahmadi, M. Ghazvini, M. Sadeghzadeh, M. Alhuyi Nazari, R. Kumar, A. Naeimi and T. Ming, "Solar power technology for electricity generation: A critical review," *Energy Sci. Eng.* **6**(5), 340–361 (2018).
- [2] G. Li, Y. Chen, Y. Yu, R. Tang and A. Mawire, "Performance and design optimization of single-axis multiposition sun-tracking PV panels," *J. Renew. Sustain. Energy* **11**(6), 063701 (2019).
- [3] Y. Zhu, J. Liu and X. Yang, "Design and performance analysis of a solar tracking system with a novel single-axis tracking structure to maximize energy collection," *Appl. Energy* **264**(8), 114647 (2020).
- [4] S. Shufat, E. Kurt and A. Hançerlioğullari, "Modeling and design of azimuth-altitude dual axis solar tracker for maximum solar energy generation," *Int. J. Renew. Energy Dev.* **8**(1), 7–13 (2019).
- [5] S. K. Natarajan, V. Thampi, R. Shaw, V. S. Kumar, R. S. Nandu, V. Jayan, N. Rajagopalan and R. K. Kandasamy, "Experimental analysis of a two-axis tracking system for solar parabolic dish collector," *Int. J. Energy Res.* **43**(2), 1012–1018 (2019).
- [6] J. Wu, B. Zhang and L. Wang, "Optimum design and performance comparison of a redundantly actuated solar tracker and its nonredundant counterpart," *Sol. Energy* **127**(5), 36–47 (2016).

- [7] X. Du, Y. Li, P. Wang, Z. Ma, D. Li and C. Wu, “Design and optimization of solar tracker with U-PRU-PUS parallel mechanism,” *Mech. Mach. Theory* **155**(1), 104107 (2021).
- [8] X. S. He, C. F. Gao, B. Wang and C. Xie, “Design and positional posture analysis of parallel sun autotracking mechanism,” *Opt. Precis. Eng.* **20**(05), 1048–1054 (2012).
- [9] Q. J. Dong, *Application Research of 3-RPS Parallel Manipulator in Sun-Tracking Photovoltaic Generation System* (Wuhan Textile University, Wuhan, 2016).
- [10] R. B. Ashith Shyam, M. Acharya and A. Ghosal, “A heliostat based on a three degree-of-freedom parallel manipulator,” *Sol. Energy* **157**(17), 672–686 (2017).
- [11] R. B. Ashith Shyam, *Design and development of a three-degree-of-freedom parallel manipulator to track the sun for concentrated solar power towers* (Indian Institute of Science, Bangalore, 2018).
- [12] T. Zheng, *Study on Lightweight Solar Concentrating and Tracking System* (Xidian University, Xi’an, 2020).
- [13] T. Zheng, F. Zheng, X. Rui, X. Ji, K. Niu and J. He, “Design and research of three-extensible-rod solar tracking drive system for photovoltaic panels,” *Adv. Eng. Sci.* **52**(02), 171–179 (2020).
- [14] X. S. Qin, L. Yang, Y. L. Hou and Y. Zhou, “Configuration and workspace analysis of a novel bionic passive spherical hinge with large workspace,” *China Mech. Eng.* **26**(3), 354–360 (2015).
- [15] F. M. Liu, C. C. Liao, Y. Y. Zhang and H. Mo, “Design and orientation workspace analysis of new dish-type solartracking platform,” *Chin. J. Eng. Des.* **29**(5), 616–626 (2022).
- [16] S. Soulayman, “Comments on solar azimuth angle,” *Renew. Energy* **123**(10), 294–300 (2018).
- [17] A. D. John and A. B. William, *Solar Engineering of Thermal Processes* (Wiley, New York, 2006).
- [18] Y. X. Tang, “Design of PID controller for high order systems based on minimum criterion of time weighted error absolute value integration,” *Electron. World* **8**(8), 110–111 (2017).
- [19] J. Kennedy and R. Eberhart, “Particle Swarm Optimization,” **In: Proceedings of ICNN’95-International Conference on Neural Networks**, vol. 4 (IEEE, 1995) pp. 1942–1948.
- [20] H. Feng, W. Ma, C. Yin and D. Cao, “Trajectory control of electrohydraulic position servo system using improved PSO-PID controller,” *Automat. Constr.* **127**(7), 103722 (2021).